BJR

Received: 20 October 2013 | Revised: 19 March 2014 | Accepted: 3 April 2014

doi: 10.1259/bjr.20130670

Cite this article as:
Zhang MQ, Sun DN, Xie YY, Peng GY, Xia J, Long HY, et al. Three-dimensional visualization of rat brain microvasculature following permanent focal ischaemia by synchrotron radiation. Br J Radiol 2014;87:20130670.

FULL PAPER

Three-dimensional visualization of rat brain microvasculature following permanent focal ischaemia by synchrotron radiation

[1]M Q ZHANG, MD, [1]D N SUN, MD, [1]Y Y XIE, MD, [2]G Y PENG, MD, [1]J XIA, MD, [1]H Y LONG, MD and [1]B XIAO, MD

[1]Department of Neurology, Xiangya Hospital, Central South University, Changsha, China
[2]Shanghai Synchrotron Radiation Facility, Shanghai Institute of Applied Physics, Chinese Academy of Sciences, Shanghai, China

Address correspondence to: Professor Bo Xiao
E-mail: *xiaobo_xy@126.com*

Objective: Identifying morphological changes that occur in microvessels under both normal and ischaemic conditions is crucial for understanding and treating stroke. However, conventional imaging techniques are not able to detect microvessels on a micron or sub-micron scale without angiography. In the present study, synchrotron radiation (SR)-based X-ray in-line phase contrast imaging (ILPCI) was used to acquire high-resolution and high-contrast images of rat brain tissues in both normal and ischaemic states.
Methods: ILPCI was performed at the Shanghai Synchrotron Radiation Facility, Shanghai, China, without the use of contrast agents. CT slices were reformatted and then converted into three-dimensional (3D) reconstruction images to analyse subtle details of the cerebral microvascular network.
Results: By using ILPCI, brain vessels up to 11.8 μm in diameter were resolved. The number of cortical and penetrating arteries detected were found to undergo a remarkable decrease within the infarct area. 3 days after permanent ischaemia, vascular masses were also observed in the peripheral region of the infarcts.
Conclusion: SR-based ILPCI-CT can serve as a powerful tool to accurately visualize brain microvasculature. The morphological parameters of blood vessels in both CT slices and 3D reconstructions were determined, and this approach has great potential for providing an effective diagnosis and evaluation for rehabilitation therapy for stroke.
Advances in knowledge: In the absence of contrast agent, the 3D morphologies of the brain microvasculature in normal and stroke rats were obtained using SR-based ILPCI. SR imaging is a sensitive and promising method which can be used to explore primary brain function.

Stroke has proved to be a predominant factor in the deterioration of the quality of life in patients and is also a major cause of death and disability worldwide. The middle cerebral artery occlusion (MCAO) model can induce focal brain infarction and replicates many of the main pathophysiological characteristics of stroke. Identifying changes in vessel microstructure is critical for elucidating the underlying pathological mechanisms. In particular, deep microvascular beds involving penetrating arteries $<100\,\mu m$ in diameter have been found to play a primary role in ischaemic disorders and haemorrhage.[1] However, conventional imaging methods, such as CT and MRI, are not sensitive enough to detect microvessels at the micron or submicron levels. Correspondingly, they have limited capabilities in providing functional information in small animal models.[2–5] Histological sections also have limitations. For example, structural overlapping of two-dimensional (2D) images can occur and the complexity of samples can be damaged during the preparation of sections. As a result, the analysis of microvessels *in vitro* is inaccurate. Thus, further development of novel micro-imaging tools is needed to improve non-invasive high-resolution imaging of microvasculature for complicated neurovascular networks under both physiological and pathological conditions.

It has recently been demonstrated that a synchrotron radiation (SR) X-ray source can provide superior high spectral resolution and small divergence, and involves the delivery of lower doses of radiation.[6] Consequently, this monochromatized X-ray source has the potential to provide a novel imaging perspective for biological and medical applications.[4–8] Owing to the weak absorption rate of soft tissues, conventional X-ray absorption imaging cannot discriminate blood vessels from surrounding structures without the use of contrast agents.[9,10] However, phase

contrast imaging (PCI), which utilizes SR technology and X-ray phase shift, is approximately 1000 times more sensitive than conventional X-ray absorption contrast imaging.[3,9,11] In particular, in-line PCI (ILPCI), a type of PCI, has been combined with CT (ILPCI-CT) to visualize the three-dimensional (3D) structures of microvessels in different organ systems. Specifically, imaging has been performed for the liver,[12] lung,[4] rat hind limb,[8] spinal cord[3] and lung cancer.[4]

In the present study, the microvasculature of rat brain under normal conditions, and also following permanent focal ischaemia induced by MCAO, was analysed using the ILPCI technique based on an SR light source. All of the experiments were performed using X-ray imaging and the biomedical application beamline (BL13W1) at the Shanghai Light Source, a new third-generation Shanghai Synchrotron Radiation Facility (SSRF) in China. The objective was to demonstrate the feasibility of obtaining and analysing 3D data for brain vasculature using the SR-ILPCI technique. Potentially, this technique can also be applied to a wide range of neurovascular pathologies.

METHODS AND MATERIALS

Experimental animals

The experimental procedures used were approved by the Animal Ethics Committee of Central South University, Changsha, China, and they are in accordance with experimental animal use and welfare requirements established by the Ministry of Health of China.

A total of 18 Sprague–Dawley® (SD) male rats (220–250 g) were used and were obtained from the Animal Center of Central South University, Changsha, China. While 3 rats were used for histological observation, the remaining 15 rats were randomly divided into three groups (5 rats per group): a normal control group, a group analysed 3 days after MCAO, and a group analysed 7 days after MCAO.

Induction of permanent focal ischaemia

A permanent MCAO model was established according to Yang et al.[13] Briefly, adult SD rats were placed in a supine position on a pad and were anaesthetized with an intraperitoneal (i.p.) injection of 10% chloral hydrate (0.4 ml kg^{-1}). Body temperature was maintained at 36.5–37.0 °C throughout the surgical procedure using a heat lamp. After the right common carotid artery was isolated, which included external and internal carotid arteries (ICA), a 4-0 nylon suture coated with silicone was inserted through the ICA to the ostium of the MCA. The mean length of the suture inserted was 18 ± 0.5 mm. The effects of occlusion were evaluated using a neurobehaviour test described by Longa et al[14] and Bederson et al[15] immediately following surgery until the rats awoke from anaesthesia following surgery.

All experimental animals were housed in acrylic box cages with free access to food and water. They were also maintained under a constant temperature (25 °C), humidity (50 ± 10%), and lighting cycle (12:12 h).

Sample preparation

All animals were deeply anaesthetized with 10% chloral hydrate (0.4 ml kg^{-1}, i.p.) prior to transcardiac perfusion. Paraformaldehyde (4%) in 0.1 M phosphate buffer (pH 7.4) was subsequently perfused at different time points. Rat brains were then extracted and fixed in a 4% paraformaldehyde solution. 24 h later, all 15 brain specimens were dehydrated using ascending gradients of ethanol and were prepared for ILPCI.

Image acquisition and post-processing

Experiments were performed using the BL13W1 beamline of the SSRF in China. The SSRF is a third-generation synchrotron source with an average beam current of 180 mA and 3.5 GeV of storage energy. The BL13W1 beamline can provide tunable photon energy that ranges from 8 to 72.5 keV. This provides a maximal target size of approximately 45 mm (horizontal) × 5 mm (vertical) at 20 keV. The distance between the samples and the downstream detector ranged from 0 to 8 m. Since the samples were fixed on a rotating stage, the sample-to-detector distance could be adjusted by moving the detector that was mounted on a rail. A camera with a charge-coupled device captured high-contrast images. A schematic of the experimental set-up for the SR imaging system at BL13W1 is shown in Figure 1. In the experiments performed, the effective pixel size of the X-ray detector was 5.9 μm.

Samples were immobile at the centre of the rotation stage. CT scanning was performed at 20.0 keV, and the sample-to-detector distance was 50 cm. A total of 720 projection images were obtained by continuously rotating samples from 0° to 180°. The exposure time was 2.5 s, and the total duration for the whole image acquisition process was approximately 35 min. In addition, five flat-field images were obtained without samples in the

Figure 1. A schematic that provides an overview of the monochromatic synchrotron radiation system for X-ray in-line phase contrast imaging at the BL13W1 beamline experimental station at the Shanghai Synchrotron Radiation Facility, Shanghai, China. Samples can be rotated from 0° to 180° to acquire sequential projection images at various angles. CCD, charge-coupled device.

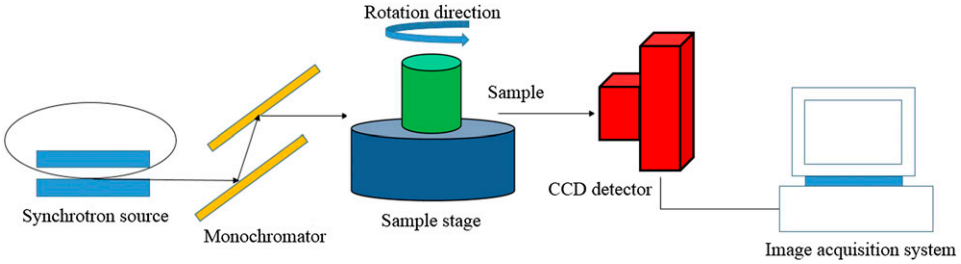

beam and five dark-field images were recorded when the light source was switched off, to subtract background signals and to eliminate small intensity discrepancies. Using a filtered back projection algorithm,[16] projection images were then reconstructed. Reformatted digital slice images were obtained using fast slice reconstruction software (supplied by BL13W1), and VG Studio Max 3D reconstruction software v. 2.1 (Volume Graphics GmbH, Heidelberg, Germany) was used to render each sequential series of CT slices into a 3D angioarchitecture image. In Figure 2, a schematic describes the procedure used to acquire CT images and the final 3D reconstruction.

Histomorphological observation

For morphological inspections of intracerebral vessels, coronal sections were obtained from three normal brains, and these were stained with haematoxylin and eosin (H&E). Intrinsic vessel images were obtained using an optical microscope (Olympus BX51; Olympus, Tokyo, Japan), and these were compared with the vascular images obtained using ILPCI-CT.

Data analysis

Diameters of visualized blood vessels were measured using National Institutes of Health Image-Pro® plus software v. 6.0 (MediaCybernetics Inc., Rockville, MD). The data are reported as the mean ± standard error.

RESULTS

Reconstructed CT slices

In Figure 3, reconstructed slices from normal control rats and their corresponding H&E-stained sections are compared. The 2D pattern of a single brain section could be observed in the ILPCI slices, whereas the histological slices had a limited visual field. The vascular distribution and structure of the hippocampus was observed in greater detail using the SR technique. The latter result is consistent with the possibility that tissue integrity was compromised as a result of sample preparation for the histological stainings. Vessels with a diameter $<50\ \mu m$ were easily discerned in the ILPCI slices, and the smallest vessels that could be discriminated had a diameter of $11.8\ \mu m$ (Figure 4). Compared with the non-infarcted side, the ischaemic region in the CT slices exhibited a reduced number and distribution of related cortical and perforating microvessels. An avascular zone was also observed at the site of the injury. 3 days after MCAO, the peripheral area of the lesions was characterized by tangled vascular channels.

Three-dimensional visualization of cerebral microvasculature

In terms of a stereoscopic effect, 3D images of the brain microvasculature were obtained using reconstructed CT slices (Figures 5–8). In Figure 5, the intact architecture of the rat brain vasculature is shown, and this includes detection of cerebral ventricles. In Figure 6, subtle details of rat brain microvasculature were observed from different angles. The gradation of colouring used in the figure indicates the natural distribution of intracerebral vessels within a certain range that was observed. Moreover, rami perforantes were present in an intertwined arrangement, thereby achieving confluence in a spatial network both horizontally and vertically. Quantification of the vessels detected showed that the average diameter of the intracerebral arteries on the proximal side was $23.6 \pm 3.3\ \mu m$ ($n = 30$). This diameter tended to gradually and narrowly extend in the spatial

Figure 2. The steps involved in the three-dimensional (3D) image reconstruction procedure. CT slices were reformatted and reconstructed using corrected original data. Various segments were then scanned and 3D digitalization was used to reconstruct the images. Integration of the images to obtain whole 3D brain images was subsequently performed.

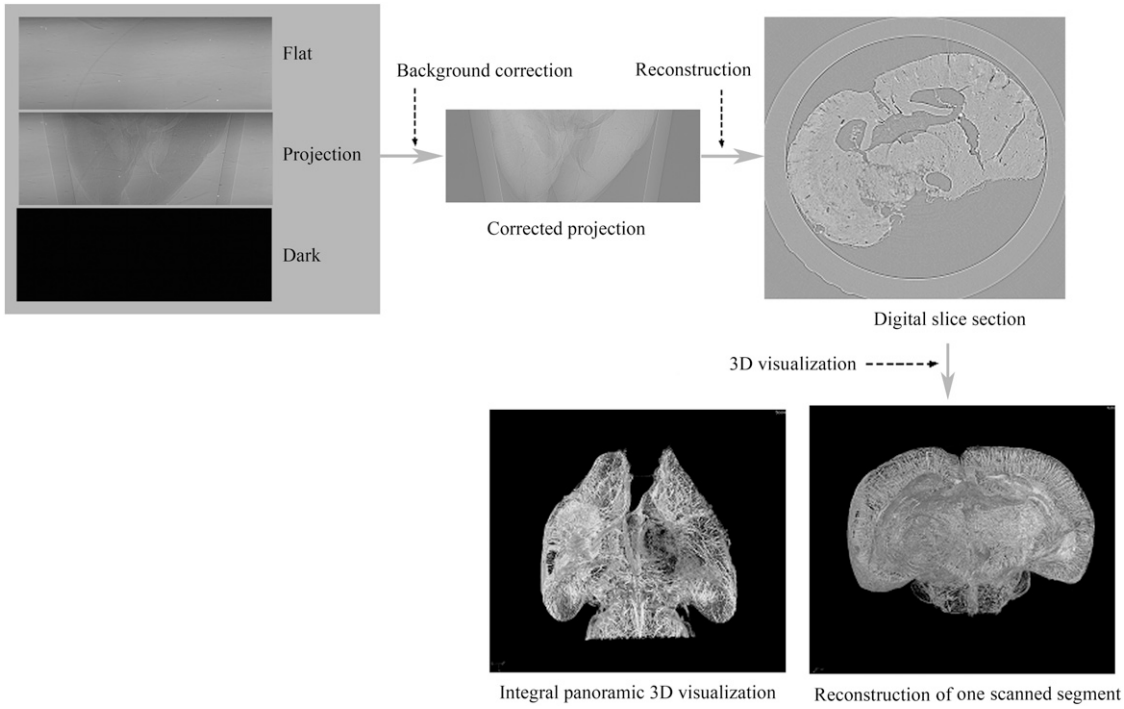

Figure 3. Histomorphological observation and reconstruction of CT slices show the angioarchitecture of the rat brain. (a) A representative slice that was reconfigured using the in-line phase contrast imaging technique. (b) Partial enlargement of (a). Vascular distribution within the hippocampus was clearly visualized. (c) Microvessel distribution within a histological section of the hippocampus. Bar = 200 μm (in a, b) and 50 μm (in c).

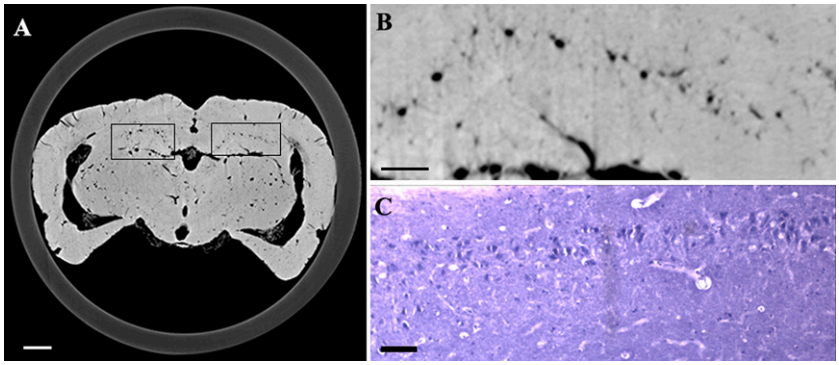

network, and, to some extent, it exceeded the limitation of the detectors. In addition, the mean interval between neighbouring deeper rami perforantes was 100.3 ± 19.7 μm ($n = 30$). The smallest vessel diameter detected was approximately 10 μm in the SR images, and this is equal to the size of a capillary.

Discrepancies did exist regarding the integral organization of the microvasculature following focal infarction. As shown in Figures 7 and 8, the number of penetrating intracerebral arteries, as well as related cortical arteries, that were observed 3 and 7 days after MCAO, respectively, exhibited a remarkable decrease on the ischaemic side compared with the contralateral side and normal brain. Primarily, collective vascular masses exhibited an irregular distribution in the peri-ischaemic region 3 days after surgery (Figure 7). At 7 days after injury, the size of the ischaemic hemisphere was smaller than that of the contralateral side (Figure 8). Although the ischaemic injury was not completely healed by Day 7 after MCAO, the avascular zone was found to have slowly constricted, potentially because of vascular healing that occurred during this time. Moreover, compared with the 3-day post-MCAO group, the cortical vessels exhibited an increasing tendency in vessel quantity.

An additional quantitative analysis was performed, with the frequency distribution of different blood vessel sizes for normal and ischaemic samples shown in Figure 9. Vessels with a diameter <20 μm were found to provide the main framework for the vasculature. 3 days after MCAO, the perfusion of vessels was found to be reduced, particularly for microvessels. Subsequently, peripheral vessels, including perforating and cortical vessels (*e.g.* <4 voxels), gradually increased in number by 7 days after MCAO. However, regarding the pattern of the larger vessels (*e.g.* >12 voxels), no distinct changes were observed between 3 and 7 days after MCAO. The latter results suggest that a steady-state self-preservation process involving larger vessels exists following MCAO injury.

DISCUSSION

To date, ischaemic stroke invariably results in severe disability and mortality, and small arteries play a key role in the primary

Figure 4. Reconstructed digital slices from the transverse view of the same position. (a) A representative CT slice from a normal rat brain with a per pixel size of 5.9 μm. Differing patterns of vessels were clearly visualized in longitudinal sections and transections. Circles are used to indicate some of the smallest microvessels that were resolved, and these were approximately 2 pixels in size. (b) A reformatted CT slice of a sample collected 3 days after middle cerebral artery occlusion (MCAO). Deep perforating vessels within the infarct region (indicated with a larger frame) disappeared, concomitant with a decrease in related cortical branches. The smaller frame is used to indicate where irregular vascular masses were observed. (c) A section obtained 7 days after MCAO. The frame indicates the infarct region. Bar = 200 μm.

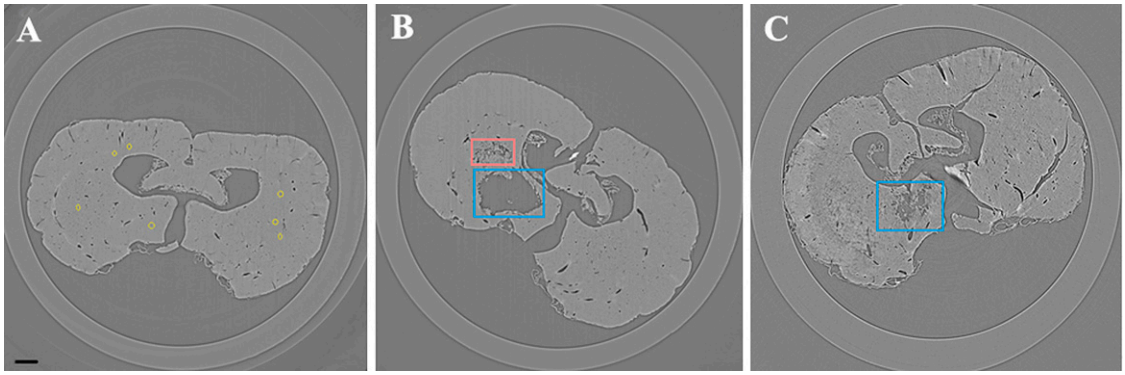

Figure 5. Three-dimensional visualization of intracerebral vasculature in normal specimens. Cerebral ventricles were revealed. A wide range of vessel diameters were detected in normal rat brain, from microvessels <20 μm in diameter to larger vessels >50 μm. Bar = 500 μm.

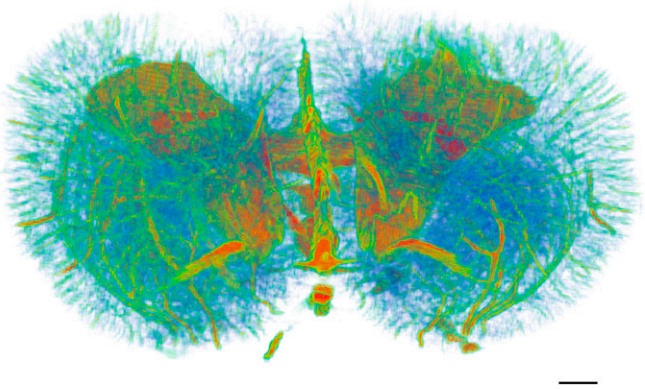

pathological changes that occur. Therefore, a better understanding of the detailed behaviour of microvasculature under physiological and pathological conditions will facilitate the early diagnosis of cerebrovascular disease, as well as the development of therapeutic interventions. Although some studies have proposed that small arteries up to 50 μm may be visualized in thick histological sections,[17] there are limitations associated with this corrosion cast method. For example, this method is invasive, requires the euthanasia of animals, and involves complex sample preparation. In addition, this method provides a limited field of view for analysis and can involve the overlapping of structures in the planar view. Taken together, these limitations make it difficult to accurately analyse intricate vascular networks using a corrosion cast method.

Imaging techniques that are currently available include MR angiography (MRA) and CT angiography. However, these methods do not provide sufficient detail in small animals.[2,3] In addition, the disadvantages of MRA include long acquisition times and the potential for flow artefacts. Furthermore, it is not a method that is well suited for evaluating acute vascular changes.[18] Regarding micro-CT, this method is able to differentiate the 3D connectivity of anatomical vasculature within intact brains. However, distribution of contrast agent(s) can affect the images obtained, and the former can be dependent on the individual perfusion and filling techniques. In addition, the micro-CT method lacks sufficient resolution to detect microvessels on a micron or submicron scale.[4] Therefore, further development of novel microimaging methods is necessary to achieve non-invasive high-resolution imaging that can detect angioarchitectural changes under physiological and pathological conditions.

SR X-rays are emitted from electrons when curvilinear movement induces a change in their direction near the speed of light. This change in direction can be controlled by a magnetic field in a storage ring[19,20] and is quite distinct from the generation of traditional X-rays following the bombardment of a metal anode with electrons. The high directionality, small divergence and variable polarization of an SR X-ray source all contribute to the acquisition of higher resolution images. Moreover, with a relatively simple set-up, SR-based ILPCI also allows sufficient amounts of coherent X-rays to propagate away from a sample, and this generates detectable phase shifts and different signal intensities. Therefore, even in the absence of contrast agent(s), this method can provide an authentic depiction of microvessel contours *ex vivo* via a boundary enhancement effect. In addition, compared with conventional histomorphology, SR images can provide details regarding the spatial architecture and volume of vascular networks.

Figure 6. Reconstruction of the three-dimensional angioarchitecture of a normal brain from different angles. (a) An apical view of the whole brain structure. (b) A lateral view of the integral vascular trees. The natural distribution of intracerebral vessels within a certain range was clearly shown. Particularly, microvessels <20 μm in diameter were a major component of the brain vasculature. Bar = 500 μm.

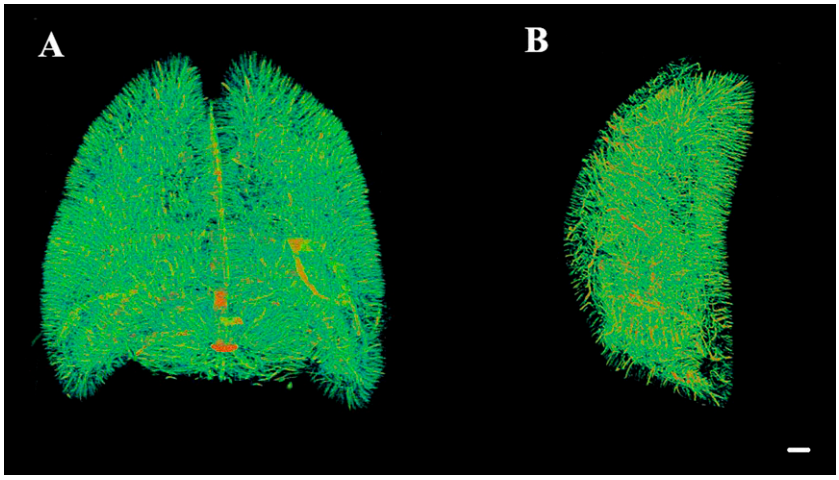

Figure 7. A three-dimensional (3D) representation of rat brain vasculature 3 days after middle cerebral artery occlusion. Imaging data were obtained from different angles, and the left-hand frame in (a) and the frames in (b) and (c) are used to show the irregular vascular network that developed in the peri-ischaemic region. (a) An apical view of the microvascular network. The left-hand frame represents the infarct region. (b) 3D images obtained from a lateral view. (c) A cross-section of the brain vasculature. Bar = 500 μm.

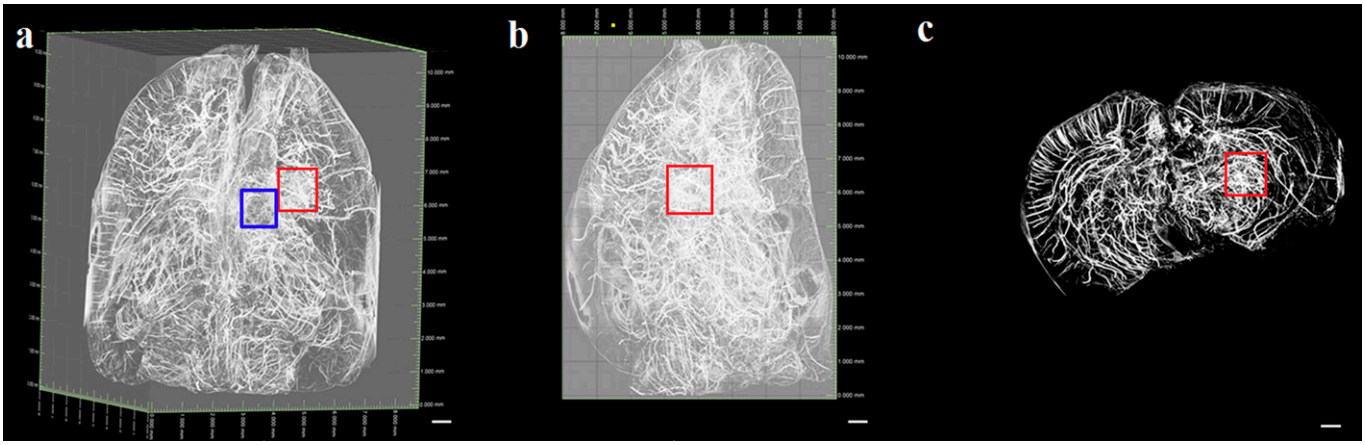

In the present study, high-resolution, high-contrast images of the rat brain vasculature were obtained using ILPCI with a per pixel size of 5.9 μm in the absence of contrast agents at the SSRF BL13W1 beamline. Reconstructed 3D angioarchitecture of the microvessel networks detected showed vascular trees were arranged in a tangled pattern that formed a network. Moreover, this network could serve to perfuse the deep parenchymal tissue. The vascular diameters measured with SR imaging were found to be consistent with data previously reported for murine brain studies.[17,21] In particular, vessels with a diameter of approximately 11.8 μm were able to be discriminated.

For rats that underwent ischaemia, the number of cortical branches and rami perforantes were found to be dramatically reduced on the lesion side. Irregularly tangled vascular masses were also observed at the periphery of the ischaemic lesions in the 3-day post-MCAO group. These peri-ischaemic changes may represent a compensative mechanism by which blood flow is improved. Alternatively, the frequency distribution of blood vessel sizes that were quantified showed that the voxel size for the smaller vessels (*e.g.* <4 voxels) gradually increased with longer post-surgery time points. For example, at the longer survival time points, the number of smaller vessels (*e.g.* <4 voxels) tended to increase. By contrast, the number of larger vessels (*e.g.* >12 voxels) was maintained and no obvious changes in the vessel number were observed during the ischaemic process. Taken together, we hypothesize that these dynamic vascular responses are involved in the vascular repair process in ischaemic brain.

Accumulating evidence indicates that ischaemic injury facilitates local angiogenesis to some extent.[22,23] Furthermore, following permanent occlusion of the MCA, endothelial cells surrounding the infarcted area have been observed to initiate proliferation as early as 12–24 h post infarct.[24] Correspondingly, an increase in vessel density was observed in the peri-infarcted region 3 days after the ischaemic insult.[25] These results are consistent with those of the present study, which indicated that the self-repair process may persist for weeks. These observations are consistent with what has been observed in 3D angiostructure analyses and

Figure 8. Three-dimensional imaging of rat brain vasculature 7 days after middle cerebral artery occlusion. The frame is used to indicate the infarct region, which appeared to exhibit malacia. Irregular vascular channels were not observed in the peri-ischaemic region. (a) An apical view of the microvascular network. (b) A cross-sectional view of the brain. Bar = 500 μm.

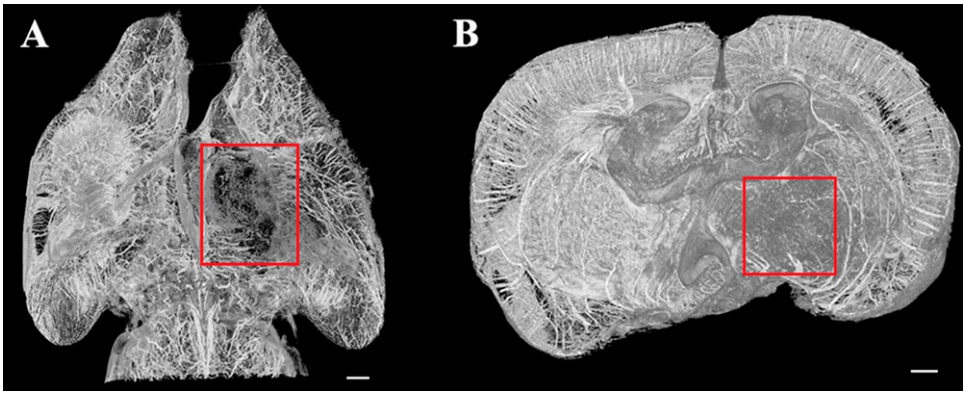

Figure 9. The frequency distribution of the blood vessel diameter index values obtained for normal and 3- and 7-day post–middle cerebral artery occlusion (MCAO) sections. The normal group exhibited a natural distribution of vessel sizes, which mainly included microvessels with diameters <4 voxels. For the MCAO groups, a reduced frequency of vessels, especially microvessels, was observed for both groups. For the 7-day post-MCAO group, perfusion was observed to gradually increase in the smaller vessels (*e.g.* <4 voxels). There was no significant difference in the number of larger vessels (*e.g.* >12 voxels) for the normal group *vs* each post-MCAO group. However, there were significant differences between the vessels with a diameter index of 4 voxels for the normal group *vs* the other two post-MCAO groups ($p < 0.05$). 1 voxel = 5.9 μm.

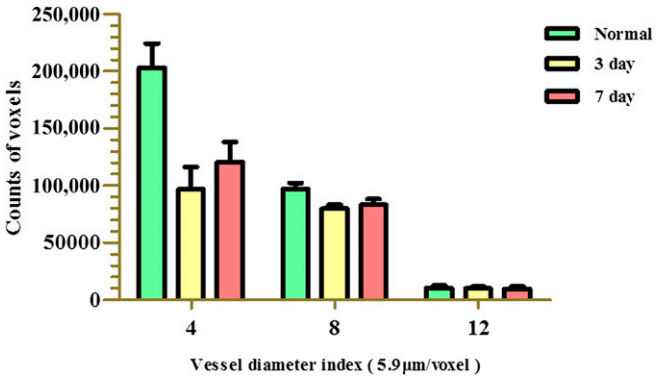

suggest that effective measures should be introduced at an early stage to further promote angiogenesis. Exogenous interventions to induce angiogenesis may also provide an opportunity to actively promote neurological recovery.[8,26] Furthermore, the use of an SR method to detect microvasculature has the potential to facilitate the evaluation of pro- or anti-angiogenesis therapeutic strategies in future studies.

It is noteworthy that the SR-ILPCI technique provides a novel and promising approach for the direct visualization of microvascular networks in the brain. Consequently, it is expected to have wide applications in the field of clinical radiology. However, ILPCI-CT does have limitations. Above all, the narrow light spot makes the imaging of large areas difficult. This is further compounded by the use of increased imaging magnification and higher resolution detectors, which reduce the field of view. Secondly, although there have been efforts to decrease the radiation doses associated with SR techniques and long exposure times, the radiation doses required for high-resolution imaging have resulted in an increase in the radiation damage experienced by biological tissues. Thirdly, ILPCI requires an X-ray source that provides high intensity, polarization, good coherence and small divergence. In fact, only an SR light source meets these strict requirements. However, the instrumentation required for SR X-ray generation and imaging may not be widely available at all biomedical institutions. Lastly, and certainly not least, shrinkage of the brain tissue as a result of the dehydration that occurs during the procedure may affect the accuracy of vessel measurements to some extent. Despite this, however, the morphology pattern of vasculature can still be completely visualized. Research is ongoing to evaluate contrast agents for SR-based ILPCI, including microbubbles.[27] While high-contrast images have been obtained with the use of novel phase contrast media, this approach may also resolve the potential for dehydration of tissues to occur. Accordingly, research is ongoing in our laboratory to characterize new tissue fixation agents to minimize the effects of the dehydration process. Admittedly, however, further development of SR facilities and techniques is needed to overcome these limitations and to provide more efficient conditions for imaging.

In addition to SR-ILPCI, SR microangiography is another novel technique that offers high-resolution, live imaging of microvasculature on a millisecond time scale. Moreover, micron-scale, real-time *in vivo* imaging of small animals is becoming more widespread. In fact, previous reports have provided imaging data for the heart,[28] kidney,[29] lung[30] and brain[5] tissues. Elleaume et al[31] performed the first human transverse coronary angiography at the European Synchrotron Radiation Facility, Grenoble, France, and images of excellent quality were obtained. The clinical application of this technology subsequently resulted in an efficient and less invasive method than conventional coronary angiography. It is anticipated that, in the near future, a combination of SR-PCI with SR microangiography will substantially increase our understanding of the changes in brain function that occur *in vivo* for several pathologies. Furthermore, we hypothesize that SR-based techniques will provide valuable insight into the functions of brain vasculature and the underlying pathological mechanisms will be elucidated for a wide range of clinical issues.

CONCLUSION

The 3D architecture of microvascular networks in the rat brain under normal and ischaemic conditions in the absence of contrast agents was obtained using SR-based ILPCI. As a result, microvessels were able to be distinguished at unprecedented resolution. Correspondingly, this technique has the potential to be a powerful tool for the comprehensive characterization of physiological and pathophysiological characteristics of vascular diseases. Furthermore, it is anticipated that future studies using SR imaging will demonstrate the capacity for this technique to provide an auxiliary diagnosis of neurovascular disorders and a more efficient evaluation of therapeutic strategies.

ACKNOWLEDGMENTS

The authors would like to thank Dr Peng Guanyun and other staff at the BL13W1 station of the Shanghai Synchrotron Radiation Facility (SSRF), Shanghai, China, for their kind assistance during the experiments.

FUNDING

This programme was completed at the BL13W1 beamline of the Shanghai Synchrotron Radiation Facility (SSRF), Shanghai, China, and was financially supported by the National Natural Science Foundation of China, Beijing, China (no. 81070941) and the Students Free Exploration Project of Central South University, Changsha, China (no. 2282013bks114).

REFERENCES

1. Phillips SJ, Whisnant JP. Hypertension and the brain. The National High Blood Pressure Education Program. *Arch Intern Med* 1992; **152**: 938–45.
2. Morita M, Ohkawa M, Miyazaki S, Ishimaru T, Umetani K, Suzuki K. Simultaneous observation of superficial cortical and intracerebral microvessels in vivo during reperfusion after transient forebrain ischemia in rats using synchrotron radiation. *Brain Res* 2007; **1158**: 116–22.
3. Hu JZ, Wu TD, Zeng L, Liu HQ, He Y, Du GH, et al. Visualization of microvasculature by x-ray in-line phase contrast imaging in rat spinal cord. *Phys Med Biol* 2012; **57**: N55–63. doi: 10.1088/0031-9155/57/5/N55
4. Liu X, Zhao J, Sun J, Gu X, Xiao T, Liu P, et al. Lung cancer and angiogenesis imaging using synchrotron radiation. *Phys Med Biol* 2010; **55**: 2399–409. doi: 10.1088/0031-9155/55/8/017
5. Liu P, Sun J, Zhao J, Liu X, Gu X, Li J, et al. Microvascular imaging using synchrotron radiation. *J Synchrotron Radiat* 2010; **17**: 517–21. doi: 10.1107/S0909049510018832
6. Zhang M, Peng G, Sun D, Xie Y, Xia J, Long H, et al. Synchrotron radiation imaging is a powerful tool to image brain microvasculature. *Med Phys* 2014; **41**: 031907. doi: 10.1118/1.4865784
7. Cai W, Gambhir SS, Chen X. Chapter 7. Molecular imaging of tumor vasculature. *Methods Enzymol* 2008; **445**: 141–76. doi: 10.1016/S0076-6879(08)03007-3
8. Lu W, Dong Z, Liu Z, Fu W, Peng Y, Chen S, et al. Detection of microvasculature in rat hind limb using synchrotron radiation. *J Surg Res* 2010; **164**: e193–9. doi: 10.1016/j.jss.2010.05.015
9. Tang R, Chai WM, Ying W, Yang GY, Xie H, Liu HQ, et al. Anti-VEGFR2-conjugated PLGA microspheres as an x-ray phase contrast agent for assessing the VEGFR2 expression. *Phys Med Biol* 2012; **57**: 3051–63. doi: 10.1088/0031-9155/57/10/3051
10. Momose A, Takeda T, Itai Y. Blood vessels: depiction at phase-contrast X-ray imaging without contrast agents in the mouse and rat—feasibility study. *Radiology* 2000; **217**: 593–6. doi: 10.1148/radiology.217.2.r00oc14593
11. Gao D, Pogany A, Stevenson AW, Wilkins SW. Phase-contrast radiography. *Radiographics* 1998; **18**: 1257–67. doi: 10.1148/radiographics.18.5.9747618
12. Duan J, Hu C, Chen H. High-resolution micro-CT for morphologic and quantitative assessment of the sinusoid in human cavernous hemangioma of the liver. *PLoS One* 2013; **8**: e53507. doi: 10.1371/journal.pone.0053507
13. Yang G, Chan PH, Chen J, Carlson E, Chen SF, Weinstein P, et al. Human copper-zinc superoxide dismutase transgenic mice are highly resistant to reperfusion injury after focal cerebral ischemia. *Stroke* 1994; **25**: 165–70.
14. Longa EZ, Weinstein PR, Carlson S, Cummins R. Reversible middle cerebral artery occlusion without craniectomy in rats. *Stroke* 1989; **20**: 84–91.
15. Bederson JB, Pitts LH, Tsuji M, Nishimura MC, Davis RL, Bartkowski H. Rat middle cerebral artery occlusion: evaluation of the model and development of a neurologic examination. *Stroke* 1986; **17**: 472–6.
16. Kak AC, Slaney M. *Principles of computerized tomographic imaging*. Philadelphia, PA: Society for Industrial and Applied Mathematics; 2001.
17. Myojin K, Taguchi A, Umetani K, Fukushima K, Nishiura N, Matsuyama T, et al. Visualization of intracerebral arteries by synchrotron radiation microangiography. *AJNR Am J Neuroradiol* 2007; **28**: 953–7.
18. Figueiredo G, Brockmann C, Boll H, Heilmann M, Schambach SJ, Fiebig T, et al. Comparison of digital subtraction angiography, micro-computed tomography angiography and magnetic resonance angiography in the assessment of the cerebrovascular system in live mice. *Clin Neuroradiol* 2012; **22**: 21–8.
19. Margaritondo G, Meuli R. Synchrotron radiation in radiology: novel X-ray sources. *Eur Radiol* 2003; **13**: 2633–41. doi: 10.1007/s00330-003-2073-7
20. Shirai M, Schwenke DO, Tsuchimochi H, Umetani K, Yagi N, Pearson JT. Synchrotron radiation imaging for advancing our understanding of cardiovascular function. *Circ Res* 2013; **112**: 209–21. doi: 10.1161/CIRCRESAHA.111.300096
21. Coyne EF, Ngai AC, Meno JR, Winn HR. Methods for isolation and characterization of intracerebral arterioles in the C57/BL6 wild-type mouse. *J Neurosci Methods* 2002; **120**: 145–53.
22. Chu K, Lee ST, Koo JS, Jung KH, Kim EH, Sinn DI, et al. Peroxisome proliferator-activated receptor-gamma-agonist, rosiglitazone, promotes angiogenesis after focal cerebral ischemia. *Brain Res* 2006; **1093**: 208–18.
23. Font MA, Arboix A, Krupinski J. Angiogenesis, neurogenesis and neuroplasticity in ischemic stroke. *Curr Cardiol Rev* 2010; **6**: 238–44. doi: 10.2174/157340310791658802
24. Hayashi T, Noshita N, Sugawara T, Chan PH. Temporal profile of angiogenesis and expression of related genes in the brain after ischemia. *J Cereb Blood Flow Metab* 2003; **23**: 166–80.
25. Beck H, Plate KH. Angiogenesis after cerebral ischemia. *Acta Neuropathol* 2009; **117**: 481–96. doi: 10.1007/s00401-009-0483-6
26. Chu M, Hu X, Lu S, Gan Y, Li P, Guo Y, et al. Focal cerebral ischemia activates neurovascular restorative dynamics in mouse brain. *Front Biosci Elite (Ed)* 2012; **4**: 1926–36.
27. Tang R, Xi Y, Chai WM, Wang Y, Guan Y, Yang GY, et al. Microbubble-based synchrotron radiation phase contrast imaging: basic study and angiography applications. *Phys Med Biol* 2011; **56**: 3503–12. doi: 10.1088/0031-9155/56/12/004
28. Umetani K, Pearson JT, Schwenke DO, Shirai M. Development of synchrotron radiation x-ray intravital microscopy for in vivo imaging of rat heart vascular function. *Conf Proc IEEE Eng Med Biol Soc* 2011; **2011**: 7791–4.
29. Eppel GA, Jacono DL, Shirai M, Umetani K, Evans RG, Pearson JT. Contrast angiography of the rat renal microcirculation in vivo using synchrotron radiation. *Am J Physiol Renal Physiol* 2009; **296**: F1023–31. doi: 10.1152/ajprenal.90499.2008
30. Schwenke DO, Pearson JT, Umetani K, Kangawa K, Shirai M. Imaging of the pulmonary circulation in the closed-chest rat using synchrotron radiation microangiography. *J Appl Physiol (1985)* 2007; **102**: 787–93. doi: 10.1152/japplphysiol.00596.2006
31. Elleaume H, Fiedler S, Esteve F, Bertrand B, Charvet AM, Berkvens P, et al. First human transvenous coronary angiography at the European Synchrotron Radiation Facility. *Phys Med Biol* 2000; **45**: L39–43.